


Article

On the Genesis of the South China Sea Mesoscale Eddies

Yuhui Zhao ¹, Yang Yang ¹ , Longjiang Mao ¹ and Yuanzhi Zhang ^{1,2,*}

¹ School of Marine Sciences, Nanjing University of Information Science and Technology, Nanjing 210044, China; 20201909002@nuist.edu.cn (Y.Z.); yangyangoceano@gmail.com (Y.Y.); mlj1214@nuist.edu.cn (L.M.)

² Center for Housing Innovations, Institute of Asia-Pacific Studies, Faculty of Social Science, Chinese University of Hong Kong, Hong Kong 999777, China

* Correspondence: yuanzhizhang@cuhk.edu.hk

Abstract: The climatology of the mesoscale eddies in the upper layer of the South China Sea (SCS) is investigated for an understanding of its genesis using the outputs from a 1/12.5° ocean reanalysis. Employed is a recently developed multiscale energetics formalism on the basis of a multiscale window transform (MWT) and the theory of canonical transfer. Three scale windows, namely, background flow, mesoscale eddy and synoptic eddy, are differentiated, and fields on different scales are reconstructed henceforth. Diagnosis of the mesoscale eddy energy budget reveals that barotropic and baroclinic instabilities, wind work, advection and pressure work are essential ingredients of the eddy energy sources and sinks in the SCS, but their contributions vary from region to region. In the southwestern part of the SCS, the regional mesoscale eddy energy is mainly generated by barotropic instability, while in the northeastern SCS, baroclinic instability and the wind working directly on the eddies are the two dominant eddy generation processes. The eddies southwest of Taiwan are damped by outward energy transport via advection, while the decay of those southeast of Vietnam is due to pressure work. The three-scale framework also reveals that the interaction between the mesoscale eddies and higher-frequency synoptic eddies mainly serves as a sink for the mesoscale eddy energy in the SCS, except for the northeastern SCS, where significant inverse cascade of kinetic energy is found.

Keywords: South China Sea; multiscale window transform; canonical transfer; multiscale energetics



Citation: Zhao, Y.; Yang, Y.; Mao, L.; Zhang, Y. On the Genesis of the South China Sea Mesoscale Eddies. *J. Mar. Sci. Eng.* **2022**, *10*, 188. <https://doi.org/10.3390/jmse10020188>

Academic Editor: Eugenio Fraile-Nuez

Received: 27 December 2021

Accepted: 26 January 2022

Published: 31 January 2022

Publisher's Note: MDPI stays neutral with regard to jurisdictional claims in published maps and institutional affiliations.



Copyright: © 2022 by the authors. Licensee MDPI, Basel, Switzerland. This article is an open access article distributed under the terms and conditions of the Creative Commons Attribution (CC BY) license (<https://creativecommons.org/licenses/by/4.0/>).

1. Introduction

The South China Sea (SCS) is the largest marginal sea in the northwestern Pacific (Figure 1). Both observations and simulations report that the surface large-scale circulation in the SCS is featured by the SCS western boundary current [1] and the Kuroshio intrusion [2]. Embedded in the large-scale currents are mesoscale eddies with scales of hundreds of kilometers and several months. It is reported that these eddies cover 9.8% of the SCS deep water area [3], serving as key contributors in transporting material and energy [4]. Statistical studies demonstrate that mesoscale eddies, though they may occur everywhere, are concentrated mainly in the southwest and the northeast in the SCS. Eddy probabilities of 40–70% southeast of Vietnam and 35–60% southwest of Taiwan, respectively, are estimated from satellite observations [5]. Correspondingly, the mesoscale eddy kinetic energy (EKE) in the SCS manifests a similar distribution as mesoscale activities, with centers of high values located southeast of Vietnam and southwest of Taiwan [6,7]. These two eddy-active regions are where strong background flows, namely the SCS western boundary and the intruded Kuroshio in the SCS, reside.

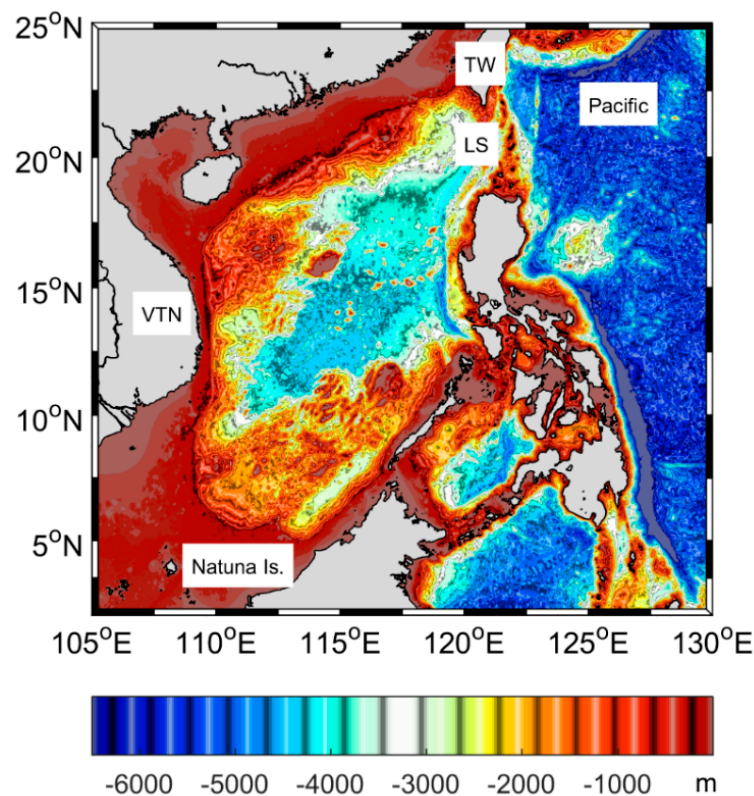


Figure 1. Topography from ETOPO1. TW, LS and VTN denote Taiwan, the Luzon Strait and Vietnam, respectively.

According to classical instability theories, the generation and development of eddies are closely related to the instability of the background flows. As far back as 1974, Gill et al. [8] showed that the available potential energy (APE) in the large-scale circulation was of the order of 1000 times the kinetic energy (KE); the abundant APE stored in the mean circulation could be released via baroclinic instability to feed eddies. This energy pathway has been confirmed in the global ocean by a variety of subsequent works (e.g., [9,10]), and also in the SCS [11]. Yang et al. [11] estimated the energy budget of mesoscale eddies in the SCS based on a high-resolution ocean general circulation model and suggested that 60% of the mesoscale eddy energy in the SCS was attributed to the release of large-scale APE via baroclinic instability. Using linear instability theory, Chen et al. [12] and Wang et al. [13] considered baroclinic instability as the dominant mechanism for the seasonal mesoscale variability in the southwestern and northeastern SCS. Compared to baroclinic instability, the role of barotropic instability, which is classically defined in association with the release of the KE of the mean flow, in governing mesoscale variability has long been overlooked. Recently, several studies revealed that barotropic instability equally participates or in some cases dominates the variability of mesoscale eddies in several ocean sectors [14–16], including the SCS [4].

In recent years, the energy cascading processes in multiscale oceanic systems have been widely investigated thanks to the rapid development of high-resolution simulations and satellite observation. Scott and Wang [17] and Scott and Arbic [18] reported a net inverse cascade from mesoscale to larger spatial scales in the ocean. These results imply that mesoscale eddies could modulate the structure and variability of the large-scale flows. In a similar way, motions with smaller scales can feed mesoscale eddies via inverse cascade. Using a $1/12^\circ$ global ocean general circulation model, Sérazin et al. [19] reported a spatiotemporal cascade from high-frequency frontal Rossby waves to the lower-frequency westward-propagating mesoscale eddies in the midlatitude North Pacific. Most recently, Yang and Liang [20] applied a novel multiscale energetics analysis tool to the Kuroshio large meander and found that during large meander events, high-frequency synoptic motions

tend to feed mesoscale eddies via inverse KE cascade. These two studies remind us to consider high-frequency synoptic eddies as a potential energy source of mesoscale eddies in the SCS.

Apart from the above-mentioned internal processes such as instabilities and scale interactions, external atmospheric forcing has long been considered as an important factor in generating mesoscale eddies. Early works (e.g., [21,22]) suggest the dominance of direct wind forcing on eddy generation in regions with low eddy activity. Subsequent studies [23–25] reveal a high correlation between wind stress and oceanic EKE in regions with weak background circulations. Recently, several studies based on satellite observations reported that wind forcing acts to damp mesoscale eddies in major western boundary currents and in the Southern Ocean as a result of wind-current effect [26,27]. As for the SCS, the wind effect on EKE is still a topic of ongoing research. A high correlation between the wind power input and the EKE southeast of Vietnam is revealed by [11], suggesting that the seasonal variability of the mesoscale eddies in that region is modulated by wind forcing. However, according to [6], most of the wind power input does not go directly into mesoscale currents in the SCS; it first drives the large-scale circulation and subsequently feeds eddies through internal instabilities.

Mesoscale eddies are active mainly in the northeast and the southwest of the SCS. The generation and development of mesoscale eddies involve complicated processes, including internal multiscale interactions and external wind effects. Previously, we investigated the seasonality of the eddy energies [28]; this study aims to give a systematic investigation of their climatology and the governing mechanisms. We use a recently developed analysis tool, namely multiscale window transform (MWT) [29], to decompose the original fields in the SCS onto three scale windows that are defined as the background flow window, the lower-frequency mesoscale eddy window and the high-frequency synoptic eddy window, respectively. Applying the MWT-based theory of canonical transfer [30], we quantitatively depict the scenario of the energy pathways, attempting to systematically explain the regional variation of the mesoscale EKE in the SCS. In Section 2, a brief introduction of the MWT and the MWT based canonical transfer theory and the dataset are provided. The main results are presented in Section 3. The study is summarized in Section 4.

2. Methods and Materials

2.1. Methodology

2.1.1. Multiscale Window Transform

Multiscale window transform (MWT) is a functional analysis tool developed by Liang and Anderson in 2007 [29]. With MWT, a function space could be orthogonally decomposed into a direct sum of several subspaces, each containing a specific range of scales which is referred to as a scale window or simply a window [29]. It is found that for a class of specially devised orthogonal filters, there exists a *localized* (here *localized* means “time-varying”, since the scale separation in this study is conducted in the frequency domain) transform-reconstruction pair which is the MWT and the multiscale window reconstruction (MWR). The MWR is analogous to a filtered field. What makes MWT different from traditional filters is that it yields a corresponding transform coefficient, which is essential to obtain the multiscale energy. Given a time series $S(t)$, the MWR on a specific scale window ω is denoted as $S^{\sim\omega}(t)$. Correspondingly, there is a transform coefficient $\hat{S}_n^{\sim\omega}$ on window ω . The localized energy on window ω proves to be $(\hat{S}_n^{\sim\omega})^2$ [29]. Note that it is by no means equal to $[S^{\sim\omega}(t)]^2$, as commonly used in literature. As mentioned in the introduction, we decompose the current system in the SCS into three scale windows which are defined as the background flow window, the mesoscale eddy window and the high-frequency synoptic eddy window. For reference convenience, the three scale windows are symbolically signified as window $\omega = 0, 1, \text{ and } 2$, respectively.

By applying MWT on both sides of the primitive equations for ocean, one can derive the energy equations on window ω . Readers may refer to [30] for more details. The KE and APE equations on window ω are as follows

$$\frac{\partial K^\omega}{\partial t} = \Gamma_K^\omega - \nabla \cdot Q_K^\omega - \nabla \cdot Q_P^\omega + b^\omega + F_K^\omega, \tag{1}$$

$$\frac{\partial A^\omega}{\partial t} = \Gamma_A^\omega - \nabla \cdot Q_A^\omega - b^\omega + F_A^\omega, \tag{2}$$

Notice the time step n is omitted for notational brevity. In the equations, $K^\omega = \frac{1}{2} \hat{\mathbf{v}}_h^{\sim\omega} \cdot \hat{\mathbf{v}}_h^{\sim\omega}$ and $A^\omega = \frac{g^2}{2\rho_0^2 N^2} (\hat{\rho}^{\sim\omega})^2$ are the multiscale KE and APE on window ω , respectively, where \mathbf{v}_h is the horizontal velocity, ρ_0 is the constant reference density ($=1025 \text{ kg/m}^3$), N is the buoyancy frequency and ρ is the density perturbation over a reference density profile (chosen as the time and area mean of the density). The terms with Hamiltonian operators, namely $-\nabla \cdot Q_K^\omega$, $-\nabla \cdot Q_A^\omega$ and $-\nabla \cdot Q_P^\omega$ stand for the divergence of KE, APE and pressure flux, respectively; b^ω represents buoyancy conversion connecting K^ω and A^ω , and the last terms on the right-hand sides are for the forcing and dissipation processes which are considered as a residue from the respective budget equations. In this study, the wind work done to the surface current on a scale window ω is also investigated, which, following [31], is expressed as $\frac{1}{\rho_0} \hat{\mathbf{v}}_0^{\sim\omega} \cdot \hat{\boldsymbol{\tau}}^{\sim\omega}$, where \mathbf{v}_0 is the surface geostrophic velocity and $\boldsymbol{\tau}$ the surface wind stress. Unlike the above processes occurring on the same scale window, the Γ terms in Equations (1) and (2) represent energy transfers across different scale windows, which is termed as canonical transfer by Liang [30].

2.1.2. Canonical Transfer Theory

Cross-scale energy transfer arising from the nonlinear advection in the momentum equation is an important process in fluid dynamics. To separate the transfer from the spatial transport process embedded in local energetics, a common practice is collecting the divergence term as the transport, and to treat the residue as the energy transfer. It has long been recognized that the transfer-transport separation is not unique, which makes the local interpretation of the scale interaction process quite ambiguous. The problem is tackled in the multiscale energetics formalism by Liang [30] who rigorously proved that a unique transfer expression can be obtained within the MWT framework. Liang proved in [30] that the transfer Γ possesses an important property:

$$\sum_\omega \sum_n \Gamma_n^\omega = 0, \tag{3}$$

which states that energy transfer is conserved in the space of scale, without generating or losing energy as a whole. Although simple to state, this property does not hold in classical energetics formalisms. To distinguish it, Γ is termed ‘‘canonical transfer’’ [31]. Canonical transfer is of key importance because it is closely related to the concept of instability in geophysical fluid dynamics. Based on the classical definition of instability (e.g., [32]), Liang [29] proved that the canonical transfers of KE and APE correspond precisely to barotropic instability and baroclinic instability, respectively.

Notice that the canonical transfer Γ^ω represents the total energy transfer from all scale windows to window ω . Through a procedure called interaction analysis [33], the canonical transfer on, for example, window 1 in a MWT framework with three scale windows, Γ^1 , can be further decomposed to obtain the window-window interactions such as $\Gamma^{0 \rightarrow 1}$ and $\Gamma^{2 \rightarrow 1}$. For a detailed derivation please refer to Section 7a in [30]. The resulting $\Gamma^{0 \rightarrow 1}$ for KE and APE (written as $\Gamma_K^{0 \rightarrow 1}$ and $\Gamma_A^{0 \rightarrow 1}$ respectively) denote the canonical transfer of KE and APE from the background flow window to the mesoscale window, respectively. Similarly, $\Gamma_K^{2 \rightarrow 1}$ and $\Gamma_A^{2 \rightarrow 1}$ denote the canonical transfers of KE and APE between the synoptic window and the mesoscale window, respectively. A positive $\Gamma_A^{0 \rightarrow 1}$ ($\Gamma_K^{0 \rightarrow 1}$) is indicative of the occurrence

of baroclinic (barotropic) instability of the background flow. The above-mentioned energy pathways within and among scale windows are schematized in Figure 2 for clarity.

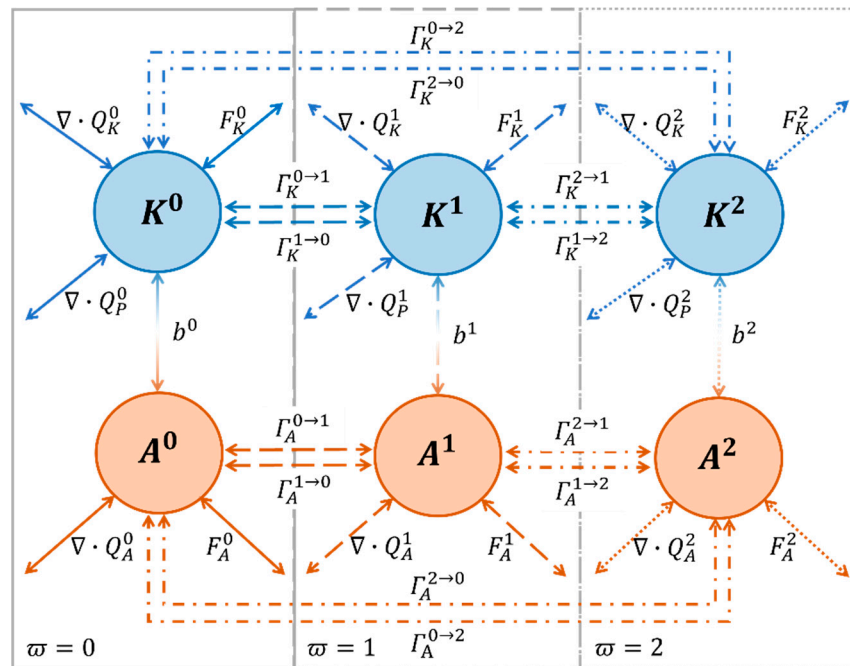


Figure 2. Schematic energy pathways in a three-scale MWT framework. Arrows of different types denote processes within and among scale windows.

2.1.3. MWT Setup

In MWT, a scale window is demarcated by scale levels. For a series with a time duration of τ , a scale level j corresponds to a period $2^{-j}\tau$. In this study, the scale levels were determined by the knowledge that the life spans of mesoscale activities in the SCS generally range from 30 to 240 days according to statistical results [3,34] and spectral analysis [28]. Therefore, we choose the mesoscale window as bounded by cutoff periods of 32 and 256 days, with their corresponding scale levels being $j_0 = 5$ and $j_1 = 8$ for $\tau = 8192$ days. By this definition, the nonstationary background flow window in this study was for motions with periods longer than 256 days, while the synoptic window was for those shorter than 32 days. The snapshots of the original SSH and geostrophic velocity fields were drawn from altimetry data, and their reconstructed fields by MWT are shown in Figure 3. This figure illustrates that the observed abundant mesoscale eddies are well separated from the background flows. Notice that the synoptic eddy window is not shown here since the merged satellite product fails to resolve most of the high-frequency signals due to its coarse resolution. Therefore, we used a high-resolution reanalysis dataset to study the eddy energetics in the SCS.

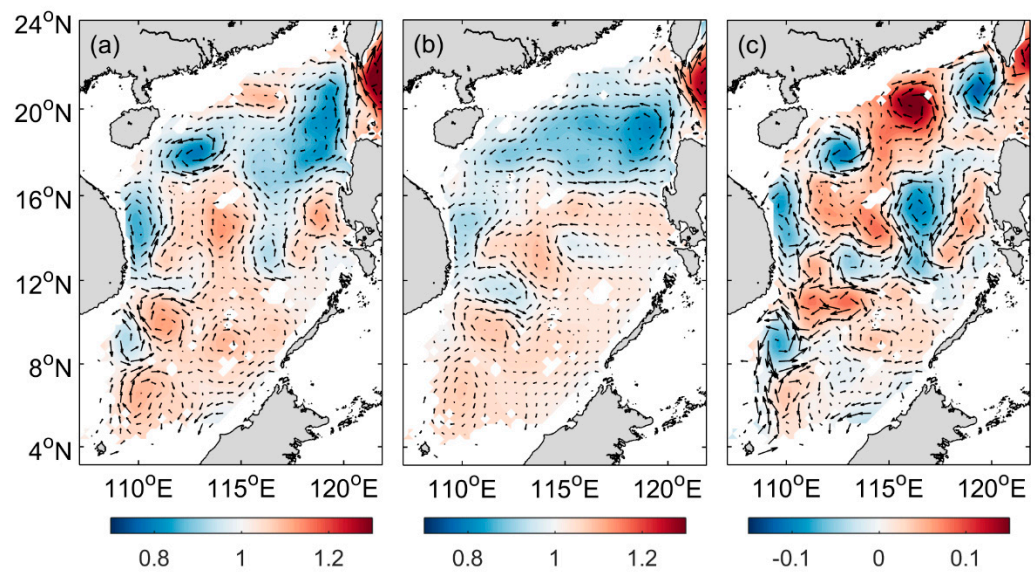


Figure 3. (a) Snapshot of the SSH (shadings; m) and geostrophic velocity (m/s) fields on 8 April 1994, from altimeter and their reconstructed fields on (b) the background flow window and (c) the mesoscale eddy window, respectively. Areas shallower than 100 m and the adjacent seas are masked to highlight the SCS.

2.2. Data

For the past few decades, the satellite measurements have greatly improved our understanding of mesoscale eddies in the global ocean. However, the satellite product is limited at the surface and therefore cannot provide the vertical structures of mesoscale activities. Besides, its coarse resolution prevents us from investigating the contribution of high-frequency processes to the mesoscale eddies. To get a full view of the energy pathway in the SCS, we use output from the Hybrid Coordinate Ocean Model (HYCOM) reanalysis (experiment GLBv0.08). The model output has a horizontal resolution of $1/12.5^\circ$ and 40 vertical levels, with the top 25 levels concentrating within the upper 300 m. It has been widely used in energetics analysis in the SCS (e.g., [35–37]). The simulation product spanning from 1994 to 2015 is selected for this study. In Section 3.1, we will show that the HYCOM reanalysis well captures the spatial characteristics of the mesoscale EKE in the SCS.

To examine the wind forcing on the SCS mesoscale eddies, we use the wind stress field offered by the USA National Centers for Environmental Prediction (NCEP) Climate Forecast System Reanalysis (CFSR) by which the HYCOM is forced. The merged product of T/P satellite altimeters provided by Archiving, Validation, and Interpretation of Satellite Oceanographic (AVISO; France) was also used as verification of the HYCOM simulation.

3. Results

3.1. Mesoscale EKE Distributions in the SCS

In this Section, we revisit the distributions of the mesoscale EKE in the SCS. Figure 4 shows the surface mesoscale EKE averaged from 1994–2015 based on the AVISO product and the HYCOM reanalysis. The observational EKE pattern (Figure 4a) confirms that the centers of strong mesoscale activities are located southwest of Taiwan and southeast of Vietnam in the SCS, consistent with previous studies [6,7]. Besides the two commonly noted regions, another region of high EKE level was found northeast of the Natuna Island where the maximum value of the averaged EKE reached $405 \text{ cm}^2/\text{s}^2$. Compared with observation, the HYCOM reanalysis well reproduces the regional mesoscale activities in the SCS, although the EKE intensities in regions southwest of Taiwan and northeast of the Natuna Island are slightly underestimated.

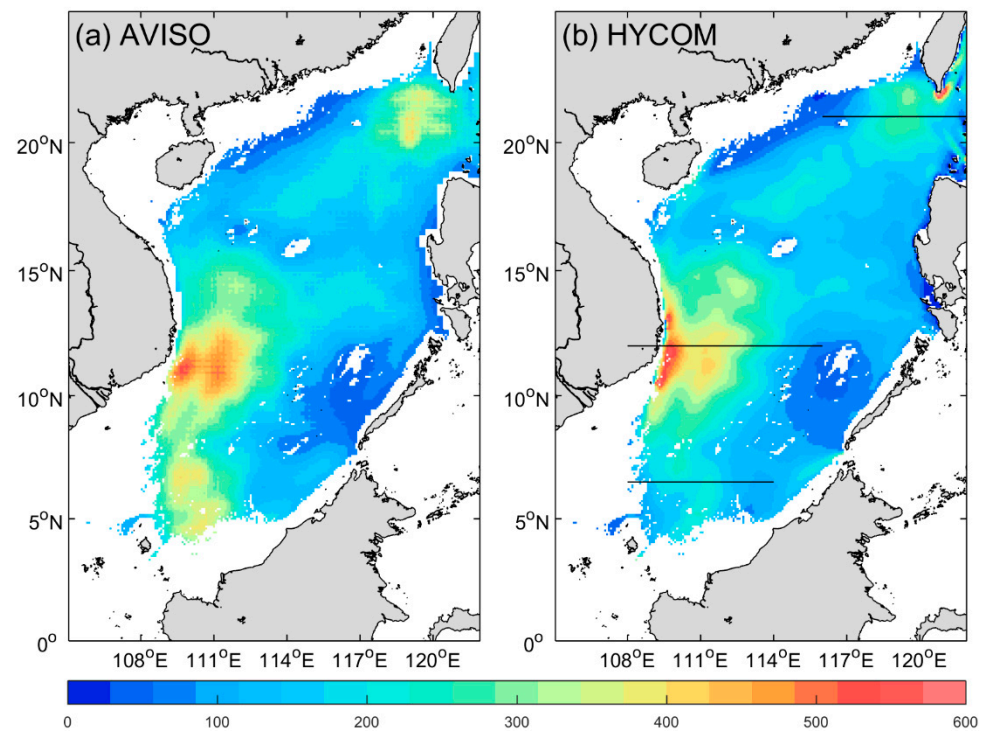


Figure 4. Surface mesoscale EKE (cm^2/s^2) estimated from (a) the AVISO product and (b) the HYCOM reanalysis. Black lines in (b) mark the sections shown in Figure 5.

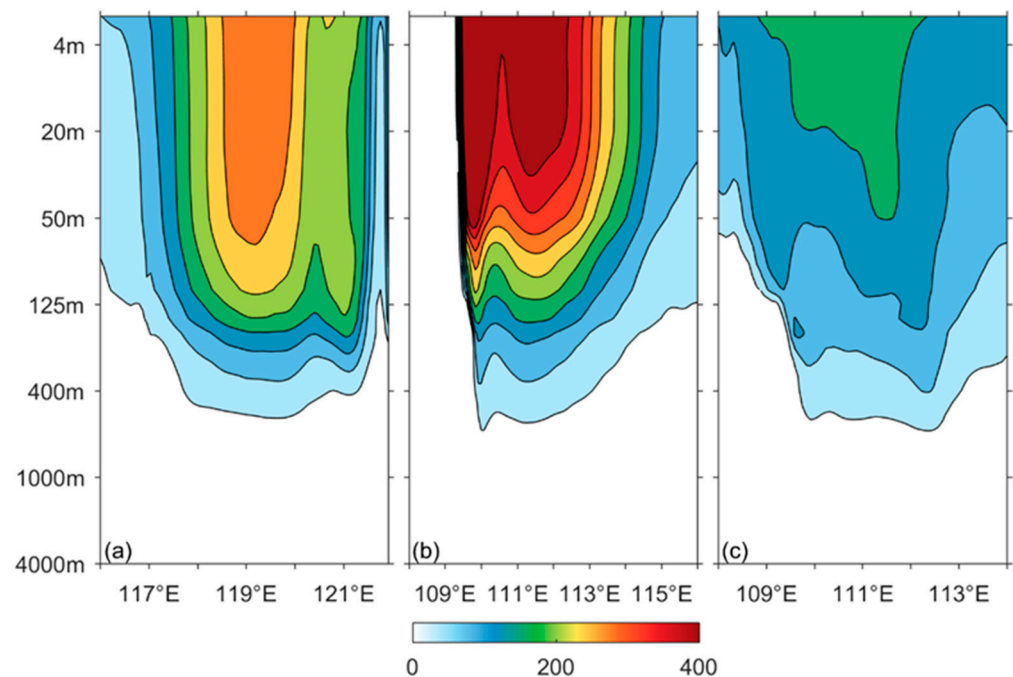


Figure 5. Vertical distributions of the mesoscale EKE (cm^2/s^2) along zonal sections (a) southwest of Taiwan, (b) southeast of Vietnam and (c) northeast of Natuna Island, respectively, as marked in Figure 4.

Using the HYCOM reanalysis data, we plotted in Figure 5 the vertical distributions of mesoscale EKE along the three zonal sections marked in Figure 4b. The locally intensified EKE manifested along the zonal direction in each region. This confirms that although the HYCOM reanalysis underestimates the mesoscale activities in these regions, it successfully reproduces the regional variation, which is of the main interest of this study. From

Figure 5, it can be seen that the EKE in the three regions are surface-intensified and decrease remarkably with depth. The region southeast of Vietnam had the largest EKE reservoir, followed by the regions southwest of Taiwan and northeast of Natuna island. Since most of the mesoscale EKE signal was confined within the upper 750 m (usually defined as the lower bound of the upper layer in the SCS), we focused on the eddy energetics within this upper layer.

3.2. Dynamics Underlying the Regional Mesoscale EKE

In Section 3.1, we identified three hotspots of mesoscale activities, located southwest of Taiwan, southeast of Vietnam and northeast of the Natuna Island, respectively. To investigate the dynamical processes responsible for this spatial variation of the mesoscale EKE in the SCS, we diagnosed the mesoscale EKE-related energy terms in Equations (1) and (2). The associated processes were classified into three categories, namely inter-scale transfers, including those from background flows and synoptic eddies to mesoscale eddies, intra-scale processes, including buoyancy conversion and nonlocal energy transport, and external wind work.

3.2.1. Inter-Scale Canonical Transfer

We first analyzed the canonical transfers from the background flow to mesoscale eddies. As introduced in Section 2.1.2, the canonical transfer of APE ($\Gamma_A^{0 \rightarrow 1}$) and KE ($\Gamma_K^{0 \rightarrow 1}$) correspond to the baroclinic instability and barotropic instability, respectively. A positive $\Gamma_A^{0 \rightarrow 1}$ ($\Gamma_K^{0 \rightarrow 1}$) indicates that the background flow is baroclinically (barotropically) unstable. Figure 6a,b display the maps of $\Gamma_A^{0 \rightarrow 1}$ and $\Gamma_K^{0 \rightarrow 1}$ vertically integrated within the upper layer. These Figures show that the three EKE maximum regions are mostly occupied by large positive values of $\Gamma_A^{0 \rightarrow 1}$ and $\Gamma_K^{0 \rightarrow 1}$, indicating that the background flow in these regions undergoes mixed baroclinic and barotropic instabilities that transfer energy to the mesoscale eddies. The forward APE transfer by baroclinic instability, as will be seen in the next section, is partly converted to KE on the mesoscale window to energize eddies. Small patches of negative $\Gamma_A^{0 \rightarrow 1}$ and $\Gamma_K^{0 \rightarrow 1}$ are also seen in the offshore regions of Taiwan and Vietnam coasts where mesoscale activities are intensive (Figure 6a,b), indicating that both APE and KE are inversely transferred from mesoscale eddies to the background flow. This suggests that other processes instead of instabilities are responsible for the EKE generation in these localized patches.

Apart from the energy transfers from background flows, those from high-frequency synoptic eddies are also analyzed. Figure 6c,d display the vertically integrated canonical transfers of APE ($\Gamma_A^{2 \rightarrow 1}$) and KE ($\Gamma_K^{2 \rightarrow 1}$) from the synoptic eddy window to the mesoscale eddy window. The two terms are overall negative in the SCS, indicating that the high-frequency synoptic eddies serve as an energy sink of the lower-frequency mesoscale eddies. However, we noticed a well-defined positive $\Gamma_K^{2 \rightarrow 1}$ pool southwest of Taiwan in which the mesoscale EKE was maximized. Such a kind of inverse KE cascade occurring in this region implies that high-frequency synoptic eddies participate in the generation and development of mesoscale eddies as a source of mesoscale KE. It should be noted that the energy transferred from the synoptic eddy window is generally an order of magnitude smaller than that from the background flow window, suggesting that the interaction between synoptic- and mesoscale eddies was relatively weak.

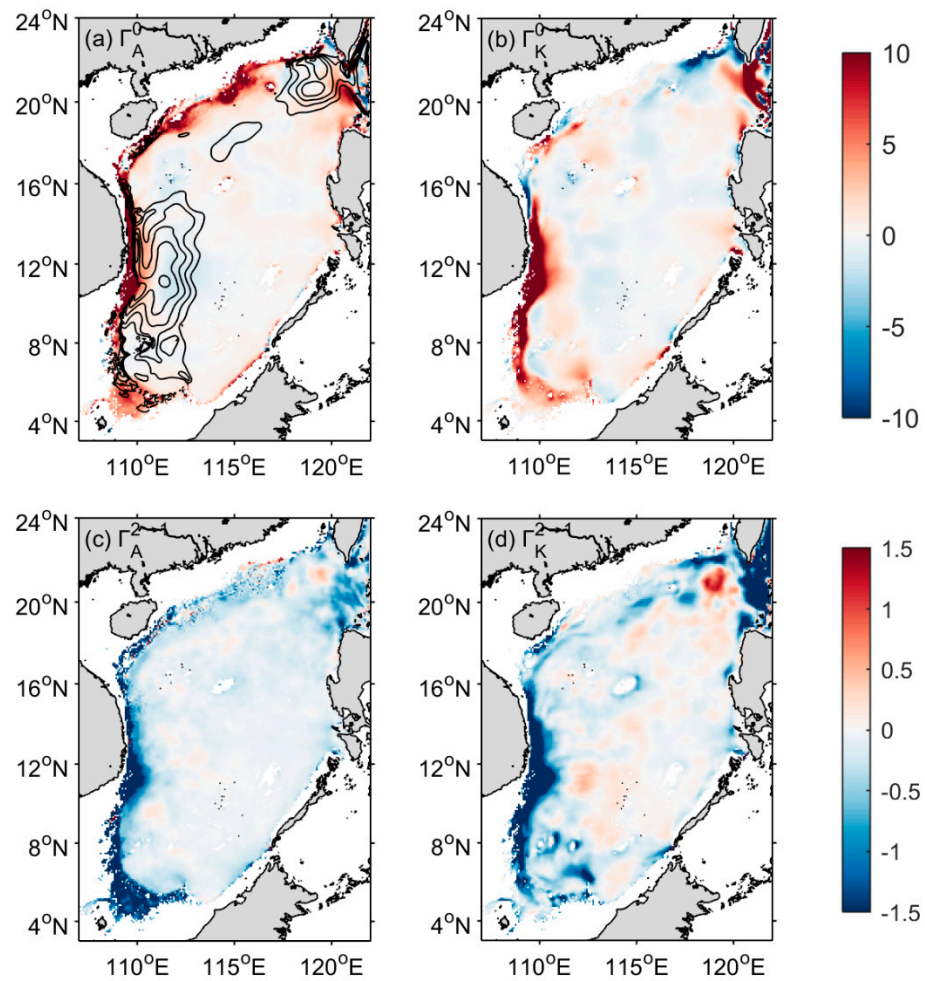


Figure 6. Horizontal maps of (a) $\Gamma_A^{0 \rightarrow 1}$, (b) $\Gamma_K^{0 \rightarrow 1}$, (c) $\Gamma_A^{2 \rightarrow 1}$ and (d) $\Gamma_K^{2 \rightarrow 1}$ integrated from surface to 750 m (shadings; cm^3/s^3). Black contours in (a) are depth-integrated mesoscale EKE with values greater than $5.5 \text{ m}^3/\text{s}^2$.

3.2.2. Intra-Scale Energy Transport and Buoyancy Conversion

As shown by the energy Equations (1) and (2), aside from the inter-scale transfers analyzed in the previous section, intra-scale processes including spatial energy transport and buoyancy conversion bridging KE and APE may also serve as energy sources in the mesoscale window. Figure 7a shows the depth-integrated convergence of KE flux on the mesoscale window, i.e., $-\nabla \cdot Q_K^1$. A positive (negative) value represents a convergence (divergence) of the mesoscale EKE. One observation from Figure 7a is that strong nonlocal processes occur along the periphery of the deep basin, especially in regions where strong EKE is observed. According to the divergence (convergence) in the nearshore (offshore) region of Vietnam coast, the direction of the mesoscale EKE transport is eastward, consistent with the flow direction of the intense Summertime Vietnam Offshore current (SVOC) in this region [38]. Recall the $\Gamma_K^{0 \rightarrow 1}$ pattern with positive (negative) values in the nearshore (offshore) region of Vietnam coast as shown in Figure 6b. The overall opposite pattern of $\Gamma_K^{0 \rightarrow 1}$ and $-\nabla \cdot Q_K^1$ suggests that the upstream SVOC undergoes barotropic instability, contributing to the strong mesoscale EKE near Vietnam. Meanwhile, part of the mesoscale EKE is transported eastward following the SVOC, leading to the high mesoscale EKE offshore. Note that the negative $\Gamma_K^{0 \rightarrow 1}$ in the offshore region was relatively small, leaving the EKE convergence as the major energy source for the vigorous mesoscale eddies there. The above result confirms the nonlocality of mesoscale eddy energy in the real ocean, consistent with a previous study by Grooms et al. [39], who reported that the eddy energy is strongly nonlocal in their two-layer quasigeostrophic simulations. A similar nonlocal

generation of mesoscale EKE was found southwest of Taiwan, as well as northeast of the Natuna Island. The $-\nabla \cdot Q_K^1$ exhibits a more complicated spatial pattern southwest of Taiwan, due to the existence of a strong Kuroshio loop current, which needs further investigation. Here, we only take the region southeast of Vietnam as an example to reveal the complex internal dynamics within a domain with high EKE levels.

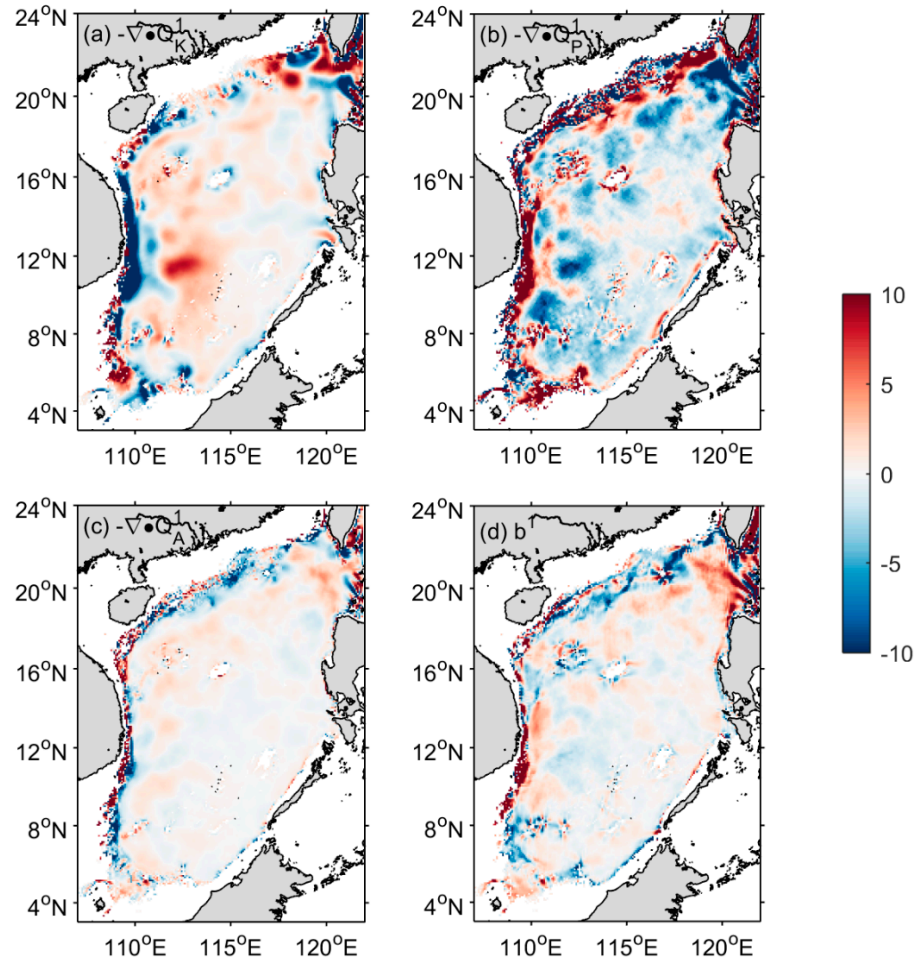


Figure 7. (a) Divergence of the KE flux, (b) divergence of the APE flux, (c) divergence of the pressure flux and (d) buoyancy conversion vertically integrated within the upper layer on the mesoscale window. The unit is cm^3/s^3 .

Figure 7b shows the horizontal distribution of the upper-layer pressure work, $-\nabla \cdot Q_P^1$, which shows a spatial pattern similar to the canonical transfers (Figure 6a,b), except in the northeastern SCS. This suggests that both pressure work and instabilities are essential mechanisms for the generation of mesoscale eddies in most areas of the SCS. Note that the amplitude of $-\nabla \cdot Q_P^1$ is comparable with, and even larger than, the canonical transfers in most areas. Recently, Quan et al. [40] reported that the dominant energy source for the intraseasonal variability in the deep layer of the SCS was pressure work. The results from [40] and this study highlight that nonlocal eddy generation by pressure work is an important factor that should be considered when investigating eddy dynamics in the SCS. Different from other regions, the contributions of $-\nabla \cdot Q_P^1$ and canonical transfers are of opposite signs in the Kuroshio loop region, suggesting that pressure work acts to redistribute the mesoscale eddy energy generated by instabilities there.

In addition to the intra-scale divergence terms appearing in the KE equation, the divergence of APE in Equation (2) was also considered, since the converged APE may be a source of KE via buoyancy conversion on the mesoscale window. A map of the upper layer divergence of the mesoscale eddy APE (EAPE), i.e., $-\nabla \cdot Q_A^1$, is displayed in

Figure 7c. It shows that the spatial transport of EAPE in the SCS is generally weak and has an irregular horizontal pattern. A large patch of positive values is seen southwest of Taiwan, indicating that the EAPE is transported from the surrounding region. The incoming EAPE by advection, together with the inter-scale APE transfer from the background flow as revealed in Section 3.2.1, are partly converted to the EKE reservoir southwest of Taiwan (see the positive buoyancy conversion, i.e., EAPE to EKE, in Figure 7d). Comparing Figure 7d with Figure 6a, we found that the buoyancy conversion and the canonical transfer of APE exhibited generally similar distributions in the upper layer. This indicated that the baroclinic instability energy pathway, namely, the APE of the background flow being released downscale to the mesoscales and further converted to EKE, was well established in most areas of the SCS.

3.2.3. Wind Work

Mesoscale eddies may also extract energy from wind stress. Figure 8a shows the mesoscale eddy wind work in the SCS. It reveals that wind stress, though inputs a large amount of KE into the mesoscales, is not always responsible for the EKE generation in the SCS. Strong eddy wind work is found in regions with low EKE levels, such as the southeast of the Luzon Strait, while weak eddy wind work corresponds to high EKE levels in several areas, such as that northeast of Natuna Island.

Besides the direct wind work done to the mesoscale eddies, another energy pathway in which wind forcing can also influence oceanic EKE is that the wind first drives the large-scale circulation, which subsequently transfers KE downscale via barotropic instability. To determine whether this scenario occurs in the SCS, we plotted in Figure 8b the wind work done on the background flow window. Intensified energy input (positive values) was observed along the western boundary as well as west of Luzon Island, where the SCS western boundary current and the intruded Kuroshio reside, confirming that the wind indeed drives the background flows. As shown in Section 3.2.1, the background flows feed energy to the mesoscale eddies through instabilities.

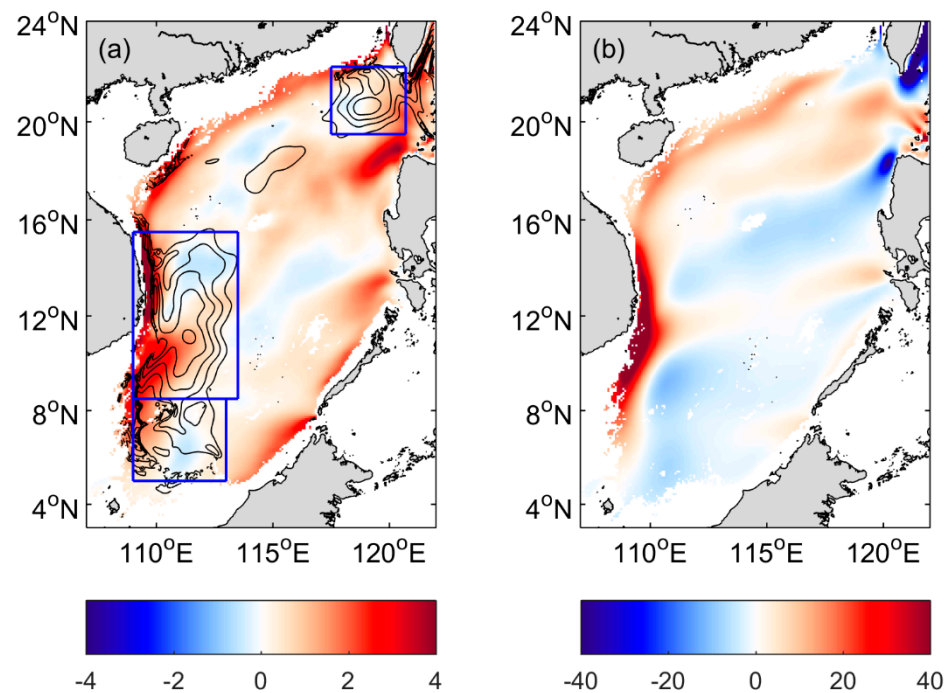


Figure 8. Work done by wind (cm^3/s^3) on (a) the mesoscale eddy window and (b) the background flow window. The integral of mesoscale EKE greater than $5.5 \text{ m}^3/\text{s}^2$ is plotted in contour in (a). The blue boxes mark the three subdomains examined in Figure 9.

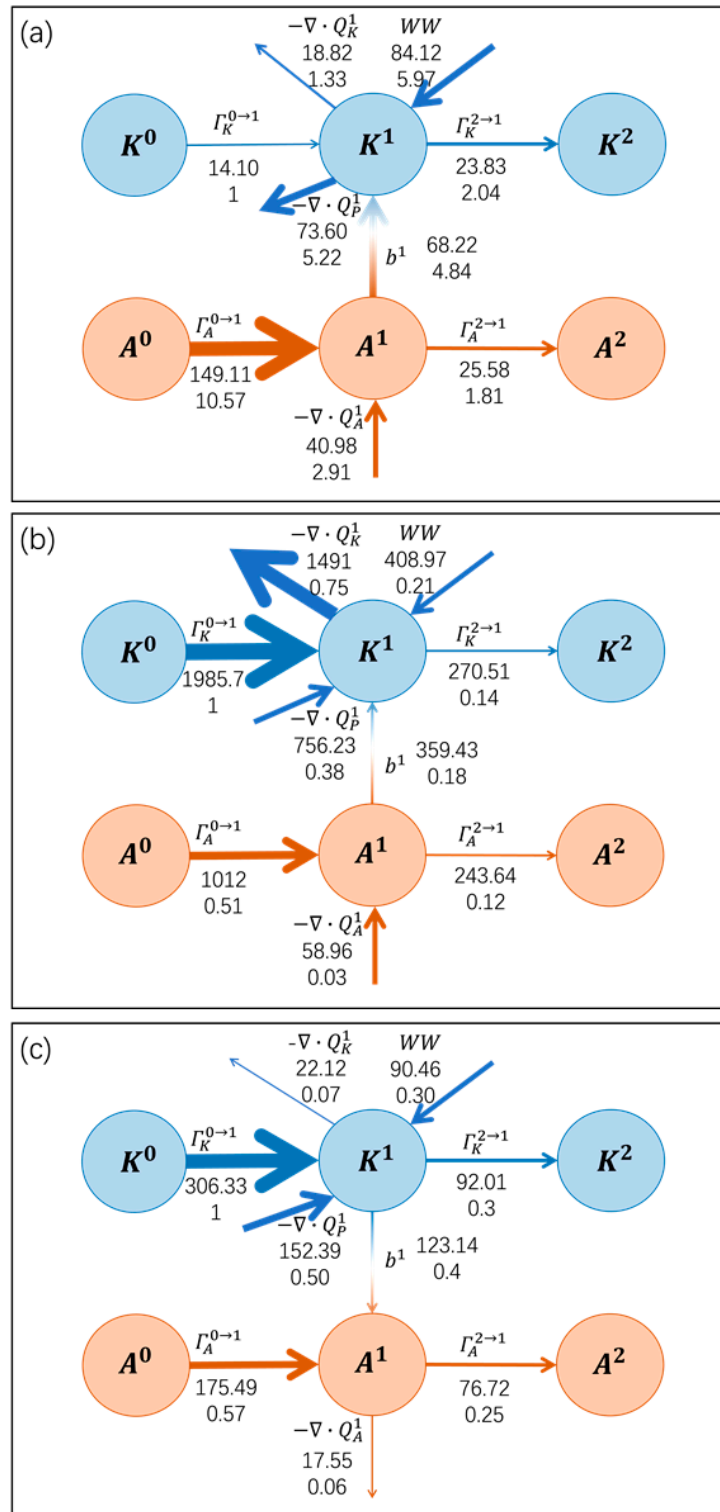


Figure 9. Schematic energy pathways (volume integration) in regions (a) southwest of Taiwan, (b) southeast of Vietnam and (c) northeast of Natuna Island. Arrows denote the energy flow directions between two reservoirs. Each term has two values that stand for the absolute value of energy flow (top) and the ratio of that term to the barotropic canonical transfer (bottom).

3.3. Energy Diagram

In Section 3.2, we investigated the internal and external processes that are responsible for the regional mesoscale EKE in the SCS. It was found that barotropic and baroclinic instabilities of the background flows, horizontal spatial energy transports and the pressure

work were key internal processes modulating the mesoscale activities in the SCS. For the external driving forcing, we found that the regional mesoscale eddies were not directly driven by the wind. Instead, the wind energy first injects into the large-scale background current, then subsequently energizes the eddies through instabilities of the background flow. Our analysis also indicates that the eddy dynamics in the northeastern SCS, where high EKE levels were observed, were quite different from those in the other two high EKE areas. To have a quantitative understanding of the different mechanisms for the regional mesoscale EKE in these subdomains, we schematized the energy pathways within the three high-EKE regions marked by the blue boxes in Figure 8a.

Figure 9a reveals that eddy wind work and baroclinic instability of the background flow ($A^0 \rightarrow A^1 \rightarrow K^1$) were the major sources for the mesoscale EKE southwest of Taiwan, while the pressure work served as the major sink. Note that although the buoyancy conversion process ($A^1 \rightarrow K^1$) converts only about half of the EAPE that is gained from large-scale APE to EKE, its contribution is much greater than that of barotropic instability ($K^0 \rightarrow K^1$). Also note that barotropic canonical transfer is an important eddy generation mechanism in this region (Section 3.2.1), although its volume integral has a relatively small value compared to the baroclinic energy pathway due to the cancellation of its negative and positive values there. Other energetic terms can be neglected due to their very small values. In contrast, barotropic instability mainly governs the strong mesoscale activities in the southwestern SCS as Figure 9b,c show. The APE release via baroclinic instability accounts for only about 35% of the mechanical energies (KE and APE) provided by the background flow, and only a small portion of the released APE is converted to the mesoscale EKE via buoyancy conversion southeast of Vietnam. Interestingly, the direction of the buoyancy conversion northeast of Natuna Island was from EKE to EAPE, leaving barotropic instability as the only EKE source in this region. Furthermore, we see from Figure 9b that the EKE advection southeast of Vietnam was the major sink of the mesoscale EKE. We also noticed that, compared with the barotropic instability of the background flow, the wind over the southwestern SCS provided a very small amount of KE for mesoscale eddies, indicating that mesoscale activities in this region are generated mainly by internal processes.

4. Conclusions

A recently developed analysis tool, multiscale window transform (MWT), as well as canonical transfer theory were used to investigate the regional mesoscale EKE in the SCS. With MWT, the original fields were decomposed onto three windows with different time scale ranges, namely the background flow window, the mesoscale eddy window, and the high-frequency synoptic eddy window. The mesoscale EKE distribution in the SCS showed three hotspots, located southwest of Taiwan, southeast of Vietnam and northeast of Natuna Island, respectively.

Based on canonical transfer theory, the energy terms in the mesoscale eddy energy equations were diagnosed. These terms correspond to three types of processes occurring in the ocean, namely, inter-scale interactions, intra-scale nonlocal transport (including EKE advection and pressure work) and buoyancy conversion, and an external process, i.e., atmospheric wind forcing. It is revealed that baroclinic and barotropic instabilities, along with the EKE advection and the pressure work jointly govern the regional mesoscale eddies in the SCS. Although the inverse cascade from high-frequency synoptic eddies transfers energies to the mesoscale eddies southwest of Taiwan and in the offshore region of Vietnam, their contribution is quite small. The wind stress inputs a large amount of KE into the mesoscale window, yet the spatial pattern of this direct wind work is not consistent with that of the EKE. Instead, we find that the wind first drives the background circulation, and subsequently energizes the mesoscale eddies through the internal processes mentioned above.

We also find that the eddy dynamics in the southwest and the northeast of the SCS have different characteristics regarding their energy pathways. In the northeastern SCS, baroclinic instability and eddy wind work are dominant in the generation and development

of mesoscale eddies, while in the southwestern SCS it is barotropic instability that accounts for the strong mesoscale EKE there. Meanwhile, the EKE divergence, advection and pressure work serve as the major sinks in regions southwest of Taiwan and southeast of Vietnam, respectively. It is worth mentioning that even inside an individual EKE hotspot, the underlying mechanisms can be different in different locations, as is shown in Section 3.2. A further detailed investigation is needed to address this issue in the future.

Author Contributions: Conceptualization, Y.Z. (Yuanzhi Zhang) and Y.Z. (Yuhui Zhao); validation, Y.Z. (Yuhui Zhao) and Y.Y.; formal analysis, Y.Z. (Yuhui Zhao) and Y.Y.; investigation, Y.Z. (Yuhui Zhao); resources, Y.Z. (Yuanzhi Zhang) and Y.Y.; data curation, Y.Z. (Yuhui Zhao); writing—original draft preparation, Y.Z. (Yuhui Zhao) and Y.Z. (Yuanzhi Zhang); writing—review and editing, Y.Y., Y.Z. (Yuanzhi Zhang) and L.M.; visualization, Y.Z. (Yuhui Zhao); supervision, Y.Z. (Yuanzhi Zhang), Y.Y., and L.M.; project administration, Y.Z. (Yuanzhi Zhang); funding acquisition, Y.Z. (Yuanzhi Zhang) and Y.Y. All authors have read and agreed to the published version of the manuscript.

Funding: This research was funded by the National Natural Science Foundation of China, grant numbers 41806023 and U1901215, and the Marine Special Program of Jiangsu Province in China (JSZRHYKJ202007).

Institutional Review Board Statement: Not applicable.

Informed Consent Statement: Not applicable.

Data Availability Statement: The results in this paper are supported by datasets including the AVISO altimeter product, HYCOM reanalysis and NCEP reanalysis. All of the datasets are publicly available. The altimeter product is available at <https://marine.copernicus.eu>. The HYCOM reanalysis and the NCEP reanalysis are available at <https://www.hycom.org>.

Acknowledgments: We thank the helpful discussions with X. San Liang, Yinchen Zhang and Weibang He about the idea of preparing the documents of this manuscript. The research was funded by the National Natural Science Foundation of China, grant numbers 41806023 and U1901215, and the Marine Special Program of Jiangsu Province in China (JSZRHYKJ202007).

Conflicts of Interest: The authors declare no conflict of interest.

References

1. Fang, G.; Wang, G.; Fang, Y.; Fang, W. A Review on the South China Sea Western Boundary Current. *Acta Oceanol. Sin.* **2012**, *31*, 1–10. [CrossRef]
2. Nan, F.; Xue, H.; Yu, F. Kuroshio Intrusion into the South China Sea: A Review. *Prog. Oceanogr.* **2015**, *137*, 314–333. [CrossRef]
3. Xiu, P.; Chai, F.; Shi, L.; Xue, H.; Chao, Y. A Census of Eddy Activities in the South China Sea during 1993–2007. *J. Geophys. Res.* **2010**, *115*, C03012. [CrossRef]
4. Ding, R.; Xuan, J.; Zhang, T.; Zhou, L.; Zhou, F.; Meng, Q.; Kang, I.-S. Eddy-Induced Heat Transport in the South China Sea. *J. Phys. Oceanogr.* **2021**, *51*, 2329–2349. [CrossRef]
5. Chen, G.; Hou, Y.; Chu, X. Mesoscale Eddies in the South China Sea: Mean Properties, Spatiotemporal Variability, and Impact on Thermohaline Structure. *J. Geophys. Res. Oceans* **2011**, *116*. [CrossRef]
6. Cheng, X.; Qi, Y. Variations of Eddy Kinetic Energy in the South China Sea. *J. Oceanogr.* **2010**, *66*, 85–94. [CrossRef]
7. Chen, G.; Hou, Y.; Chu, X.; Qi, P.; Hu, P. The Variability of Eddy Kinetic Energy in the South China Sea Deduced from Satellite Altimeter Data. *Chin. J. Oceanol. Limnol.* **2009**, *27*, 943–954. [CrossRef]
8. Gill, A.E.; Green, J.S.A.; Simmons, A.J. Energy Partition in the Large-Scale Ocean Circulation and the Production of Mid-Ocean Eddies. *Deep Sea Res. Oceanogr. Abstr.* **1974**, *21*, 499–528. [CrossRef]
9. Ferrari, R.; Wunsch, C. Ocean Circulation Kinetic Energy: Reservoirs, Sources, and Sinks. *Annu. Rev. Fluid Mech.* **2009**, *41*, 253–282. [CrossRef]
10. von Storch, J.-S.; Eden, C.; Fast, I.; Haak, H.; Hernández-Deckers, D.; Maier-Reimer, E.; Marotzke, J.; Stammer, D. An Estimate of the Lorenz Energy Cycle for the World Ocean Based on the STORM/NCEP Simulation. *J. Phys. Oceanogr.* **2012**, *42*, 2185–2205. [CrossRef]
11. Yang, H.; Wu, L.; Liu, H.; Yu, Y. Eddy Energy Sources and Sinks in the South China Sea. *J. Geophys. Res. Ocean* **2013**, *118*, 4716–4726. [CrossRef]
12. Chen, G.; Gan, J.; Xie, Q.; Chu, X.; Wang, D.; Hou, Y. Eddy Heat and Salt Transports in the South China Sea and Their Seasonal Modulations. *J. Geophys. Res.* **2012**, *117*. [CrossRef]
13. Wang, H.; Wang, D.; Liu, G.; Wu, H.; Li, M. Seasonal Variation of Eddy Kinetic Energy in the South China Sea. *Acta Oceanol. Sin.* **2012**, *31*, 1–15. [CrossRef]

14. Yang, Y.; Liang, X.S. On the Seasonal Eddy Variability in the Kuroshio Extension. *J. Phys. Oceanogr.* **2018**, *48*, 1675–1689. [[CrossRef](#)]
15. Kang, D.; Curchitser, E.N.; Rosati, A. Seasonal Variability of the Gulf Stream Kinetic Energy. *J. Phys. Oceanogr.* **2016**, *46*, 160224111526006. [[CrossRef](#)]
16. Jouanno, J.; Sheinbaum, J.; Barnier, B.; Molines, J.M.; Candela, J. Seasonal and Interannual Modulation of the Eddy Kinetic Energy in the Caribbean Sea. *J. Phys. Oceanogr.* **2012**, *42*, 2041–2055. [[CrossRef](#)]
17. Scott, R.B.; Wang, F. Direct Evidence of an Oceanic Inverse Kinetic Energy Cascade from Satellite Altimetry. *J. Phys. Oceanogr.* **2005**, *35*, 1650–1666. [[CrossRef](#)]
18. Scott, R.B.; Arbic, B.K. Spectral Energy Fluxes in Geostrophic Turbulence: Implications for Ocean Energetics. *J. Phys. Oceanogr.* **2007**, *37*, 673–688. [[CrossRef](#)]
19. Sérazin, G.; Penduff, T.; Barnier, B.; Molines, J.-M.; Arbic, B.K.; Müller, M.; Terray, L. Inverse Cascades of Kinetic Energy as a Source of Intrinsic Variability: A Global OGCM Study. *J. Phys. Oceanogr.* **2018**, *48*, 1385–1408. [[CrossRef](#)]
20. Yang, Y.; Liang, X.S. New Perspectives on the Generation and Maintenance of the Kuroshio Large Meander. *J. Phys. Oceanogr.* **2019**, *49*, 2095–2113. [[CrossRef](#)]
21. Frankignoul, C.; Müller, P. Quasi-Geostrophic Response of an Infinite β -Plane Ocean to Stochastic Forcing by the Atmosphere. *J. Phys. Oceanogr.* **1979**, *9*, 104–127. [[CrossRef](#)]
22. Müller, P.; Frankignoul, C. Direct Atmospheric Forcing of Geostrophic Eddies. *J. Phys. Oceanogr.* **1981**, *11*, 287–308. [[CrossRef](#)]
23. Garnier, V.; Schopp, R. Wind Influence on the Mesoscale Activity along the Gulf Stream and the North Atlantic Currents. *J. Geophys. Res.* **1999**, *104*, 18087–18110. [[CrossRef](#)]
24. Stammer, D.; Böning, C.; Dieterich, C. The Role of Variable Wind Forcing in Generating Eddy Energy in the North Atlantic. *Prog. Oceanogr.* **2001**, *48*, 289–311. [[CrossRef](#)]
25. Brachet, S. Mesoscale Variability from a High-Resolution Model and from Altimeter Data in the North Atlantic Ocean. *J. Geophys. Res.* **2004**, *109*, C12025. [[CrossRef](#)]
26. Xu, C.; Zhai, X.; Shang, X.-D. Work Done by Atmospheric Winds on Mesoscale Ocean Eddies: Wind work on ocean eddies. *Geophys. Res. Lett.* **2016**, *43*, 12174–12180. [[CrossRef](#)]
27. Renault, L.; McWilliams, J.C.; Masson, S. Satellite Observations of Imprint of Oceanic Current on Wind Stress by Air-Sea Coupling. *Sci Rep.* **2017**, *7*, 17747. [[CrossRef](#)]
28. Zhao, Y.; Yang, Y.; Liang, X.S.; Zhang, Y. Different Mechanisms for the Seasonal Variations of the Mesoscale Eddy Energy in the South China Sea. *Deep Sea Res. Part I Oceanogr. Res. Pap.* **2021**, *179*, 103677. [[CrossRef](#)]
29. Liang, X.S.; Anderson, D.G.M. Multiscale Window Transform. *Multiscale Model. Simul.* **2007**, *6*, 437–467. [[CrossRef](#)]
30. Liang, X.S. Canonical Transfer and Multiscale Energetics for Primitive and Quasigeostrophic Atmospheres. *J. Atmos. Sci.* **2016**, *73*, 4439–4468. [[CrossRef](#)]
31. Wunsch, C. The Work Done by the Wind on the Oceanic General Circulation. *J. Phys. Oceanogr.* **1998**, *28*, 2332–2340. [[CrossRef](#)]
32. Pedlosky, J. *Geophysical Fluid Dynamics*; Springer: Berlin/Heidelberg, Germany, 1979; p. 624.
33. Liang, X.S.; Robinson, A.R. Localized Multiscale Energy and Vorticity Analysis. *Dyn. Atmos. Oceans* **2005**, *38*, 195–230. [[CrossRef](#)]
34. Zhang, M.; von Storch, H.; Chen, X.; Wang, D.; Li, D. Temporal and Spatial Statistics of Travelling Eddy Variability in the South China Sea. *Ocean Dyn.* **2019**, *69*, 879–898. [[CrossRef](#)]
35. Zhao, Y.B.; Liang, X.S.; Gan, J. Nonlinear Multiscale Interactions and Internal Dynamics Underlying a Typical Eddy-Shedding Event at Luzon Strait: Luzon Eddy-Shedding Dynamics. *J. Geophys. Res. Oceans* **2016**, *121*, 8208–8229. [[CrossRef](#)]
36. Zhang, Z.; Zhao, W.; Qiu, B.; Tian, J. Anticyclonic Eddy Sheddings from Kuroshio Loop and the Accompanying Cyclonic Eddy in the Northeastern South China Sea. *J. Phys. Oceanogr.* **2017**, *47*, 1243–1259. [[CrossRef](#)]
37. Quan, Q.; Cai, Z.; Jin, G.; Liu, Z. Topographic Rossby Waves in the Abyssal South China Sea. *J. Phys. Oceanogr.* **2021**, *51*, 1795–1812. [[CrossRef](#)]
38. Li, Y.; Han, W.; Wilkin, J.L.; Zhang, W.G.; Arango, H.; Zavala-Garay, J.; Levin, J.; Castruccio, F.S. Interannual Variability of the Surface Summertime Eastward Jet in the South China Sea. *J. Geophys. Res. Oceans* **2014**, *119*, 7205–7228. [[CrossRef](#)]
39. Grooms, I.; Nadeau, L.-P.; Smith, S. Mesoscale Eddy Energy Locality in an Idealized Ocean Model. *J. Phys. Oceanogr.* **2013**, *43*, 1911–1923. [[CrossRef](#)]
40. Quan, Q.; Liu, Z.; Sun, S.; Cai, Z.; Yang, Y.; Jin, G.; Li, Z.; Liang, X.S. Influence of the Kuroshio Intrusion on Deep Flow Intraseasonal Variability in the Northern South China Sea. *J. Geophys. Res. Oceans* **2021**, *126*, e2021JC017429. [[CrossRef](#)]